3D Acoustic Streaming Field in High-Intensity Discharge Lamps

Bernd Baumann*[1], Joerg Schwieger[1], Marcus Wolff[1], Freddy Manders[2], and Jos Suijker[2,3]

[1]Hamburg University of Applied Sciences, Germany, [2]Philips Lighting, Belgium, [3]Technical University Eindhoven, Netherlands
* Corresponding author: Heinrich Blasius Institute for Physical Technologies, Department of Mechanical Engineering and Production, Hamburg University of Applied Sciences, Berliner Tor 21, 20099 Hamburg, Germany, info@BerndBaumann.de

Abstract: For the reasons of energy efficiency and material cost reduction one would prefer to drive high-intensity discharge lamps at frequencies of about 300 kHz. Operating lamps at these high frequencies bears the risk of stimulating acoustic resonances inside the arc tube, which can result in low frequency light flicker and even lamp destruction. The acoustic streaming effect has been identified as the link between the high frequency resonances and the low frequency flicker. A highly coupled 3D multiphysics model has been set up to calculate the acoustic streaming velocity field inside the arc tube of high-intensity discharge lamps. This velocity field is an important quantity for the understanding of the lamp behavior and a prerequisite for a forthcoming linear stability analysis, which will be used to identify light flicker.

Keywords: Acoustic resonance, acoustic streaming, lighting, plasma

1 Introduction

Worldwide 19% of the electric power is consumed for lighting [1, 2]. A considerable fraction of artificial light sources are high-intensity discharge (HID) lamps which are used for outdoor lighting, shop lighting, automobile headlights and other applications. Despite an increasing market share of light emitting diodes, HID lamps will be irreplaceable in the foreseeable future because of their superior color rendering index and their sun like luminance [3]. Although HID lamps have reached a certain stage of technical maturity, further effort is required in order to obtain lamps of highest quality and efficiency.

The design of the lamp investigated in this article is depicted in the left part of Figure 1. A voltage applied to the electrodes inside the arc tube establishes a plasma arc, which constitutes the source of light emission. To avoid electrode erosion and demixing of the arc tube filling, HID lamps are operated with alternating current (AC). From the electronic point of view minimal material costs are achieved at the energetically optimal operation frequency of approximately 300 kHz [4]. Unfortunately, in this frequency range periodic heating due to ohmic loss excites acoustic resonances. The high frequency sound wave, however, causes a low frequency movement (ca. 10 Hz) of the plasma arc that is visible as light flicker (Figure 1, right). It has recently been discovered that the acoustic streaming (AS) phenomenon is responsible for this link [5]. For further improvement of the lamp design a thorough understanding of the underlying mechanisms is crucial. Here we present results obtained with a stationary 3D finite element model for the calculation of the streaming field. As a test case we chose the moderate frequency resonance at 47.4 kHz.

2 Model

2.1 Temperature Field

The investigation of light flicker in HID lamps requires a model that comprises a number of coupled equations that describe the processes inside the arc tube, the arc tube's wall and the electrodes. In contrast to the time-dependent 2D model of [6] that describes an arc tube of infinite length, we use a stationary 3D model. Arc flicker shall be identified through instabilities of the velocity field.

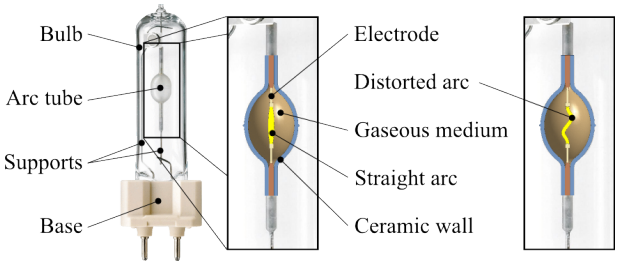

Figure 1: Left: Design of the investigated HID lamp (Philips 35 W 930 Elite). The arc tube contains mainly argon, mercury and metal halides. The arc tube is made from polycrystalline alumina (PCA). The distance between the tungsten electrodes is 4.8 mm. Right: Arc perturbation in vertical lamp operation.

The electric potential ϕ is determined from the equation of charge conservation:

$$\vec{\nabla} \cdot \left(\sigma \vec{E}\right) = 0.$$

$\vec{E} = -\vec{\nabla}\phi$ is the electric field and σ the temperature dependent electric conductivity (see the table in the appendix and Figure 2). The buoyancy driven velocity field $\vec{u}$ is calculated from the Navier-Stokes equation

$$\rho\left(\vec{u}\cdot\vec{\nabla}\right)\vec{u} = \vec{f} + \vec{\nabla}\cdot\left[-P\mathbf{I} + \eta\left(\vec{\nabla}\vec{u} + \left(\vec{\nabla}\vec{u}\right)^{\mathrm{T}}\right) - \frac{2}{3}\eta\left(\vec{\nabla}\cdot\vec{u}\right)\mathbf{I}\right]$$

in combination with the equation describing mass conservation

$$\vec{\nabla}\cdot(\rho\vec{u}) = 0$$

(ρ density, P pressure inside arc tube, η dynamic viscosity). The Cartesian components of the buoyancy force

$$f_l = -\delta_{l3}\rho g$$

(δ_{l3} Kronecker symbol, $g = 9.81\ \mathrm{m/s^2}$) bends the plasma arc upward off the symmetry axis when the lamp is operated horizontally. This loss of symmetry enforces the use of a 3D model. The temperature field T inside the arc tube is determined from the Elenbaas-Heller equation

$$\vec{\nabla}\cdot\left(-\kappa\vec{\nabla}T\right) + \rho c_p\vec{u}\cdot\vec{\nabla}T = \sigma|\vec{E}|^2 - q_{\mathrm{rad}}$$

(κ thermal conductivity, c_p heat capacity at constant pressure, q_{rad} power loss density due to radiation). The domain of the Elenbaas-Heller equation comprises the inside of the arc tube, the electrodes and the wall. The differential equations have to be supplemented by boundary conditions. These can be found in Figure 3.

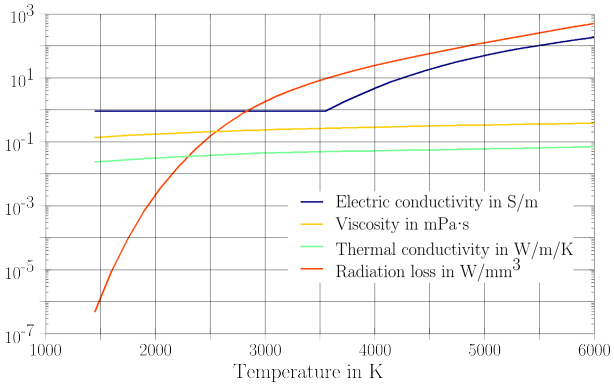

Figure 2: Temperature dependency of some material properties. To account for deviations from local thermal equilibrium of the electric conductivity, a temperature-independent electric conductivity is used below a temperature threshold of 3550 K [7].

The equations above serve for the calculation of the temperature distribution inside the arc tube, which are necessary for the calculation of the acoustic pressure.

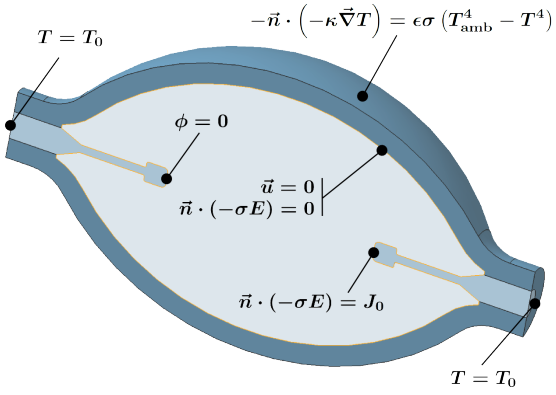

Figure 3: Boundary conditions for differential equations of section 2.1.

2.2 Acoustic Pressure

To obtain the acoustic pressure p inside the arc tube we need to solve the inhomogeneous Helmholtz equation

$$\vec{\nabla}\left(\frac{1}{\rho}\vec{\nabla}p\right) + \frac{\omega^2}{\rho c^2}p = \mathrm{i}\omega\frac{\gamma-1}{\rho c^2}\mathcal{H}$$

under the assumption that the walls of the arc tube are sound hard. The density ρ as well as the speed of sound c are temperature- and, therefore, space-dependent quantities[1]. γ is the ratio of the heat capacities and $\mathcal{H}$ the power density of heat generation. In the present context we have

$$\mathcal{H} = \sigma|\vec{E}|^2 - q_{\mathrm{rad}}.$$

The inhomogeneous Helmholtz equation can be solved by an eigenmode expansion of the acoustic pressure [8, 9]:

$$p(\vec{r},\omega) = \sum_j A_j(\omega)p_j(\vec{r}).$$

The eigenmodes are obtained by solving the homogeneous Helmholtz equation and normalize the solutions according to

$$\int_{V_\mathrm{C}} p_i^* p_j \,\mathrm{d}V = V_\mathrm{C}\delta_{ij}$$

(V_C is the volume enclosed by the walls of the arc tube). In this article the pressure at one of the resonance frequencies ω_j is of interest. Under the assumption that the eigenfrequencies are fairly separated to each other the series above reduces to one term:

$$p(\vec{r},\omega_j) \approx A_j(\omega_j)p_j(\vec{r}).$$

The amplitude can be calculated from

$$A_j(\omega_j) = \frac{(\gamma-1)}{\omega_j L_j V_\mathrm{C}}\int_{V_\mathrm{C}} p_j^*\mathcal{H}\,\mathrm{d}V,$$

where L_j is the loss factor. How to estimate the loss factor is described in [10]. Here we only consider volume loss due to heat conduction and viscosity, as well as surface loss due to heat conduction and viscosity.

[1] Actually $c\rho^2$ is constant

2.3 Streaming Field

Everybody is used to the fact that a fluid streaming around a rigid structure can produce noise. Less common is the knowledge of the opposite effect: Noise can produce fluid flow with a non vanishing time average of mass transport. When this happens, one speaks of acoustic streaming [11]. From the mathematical point of view it is a nonlinear second order effect.

If a standing pressure wave is excited in a closed vessel like the arc tube of an HID lamp, the particles of the fluid experience a viscous force in particular near the wall. The particles in immediate neighborhood of the wall are at rest and cannot participate in the oscillation (no slip boundary condition). The viscosity induces a vortex-like motion of the arc tube filling inside the viscous boundary layer (inner streaming) [12]. Simultaneously, a second vortex-like motion is generated outside the boundary layer (outer streaming or Rayleigh streaming) [12]. The size of the vortexes connected to outer streaming is of the order of the wavelength of the standing pressure wave. Arc flicker is caused by the outer streaming vortexes [5].

To obtain the streaming field, one has to solve the Navier-Stokes equation once more. The force density is now

$$f_l = \frac{\partial\overline{\rho v_k v_l}}{\partial x_k} - \delta_{l3}\rho g.$$

Here Einstein's sum convention and time averaging over one cycle is understood. $\vec{v}$ is the sound particle velocity. For time harmonic waves the force density can be expressed by the amplitude $\hat{\vec{v}}$ of the sound particle velocity

$$f_l = \frac{1}{2}\frac{\partial\rho\hat{v}_k\hat{v}_l}{\partial x_k} - \delta_{l3}\rho g,$$

which can be calculated from the acoustic pressure via [13]

$$\hat{\vec{v}}(\vec{r},\omega_j) = \frac{1}{\mathrm{i}\omega_j\rho}\vec{\nabla}p(\vec{r},\omega_j) = \frac{A_j(\omega_j)}{\mathrm{i}\omega_j\rho}\vec{\nabla}p_j(\vec{r}).$$

Using the acoustic pressure modes from Section 2.2 for the calculation of the sound particle velocity is not sufficient for the determination of the streaming field. The reason is that the eigenmodes of the Helmholtz equation do not account for the no slip condition at the boundaries, which is essential for the formation of the streaming vortices. In [14] one can find a solution to this problem. The

sound particle velocity has to be multiplied by a factor that is equal to one almost everywhere inside the arc tube and drops to zero at the wall:

$$\hat{v}_k(\vec{r},\omega_j) \to \hat{v}_k^*(\vec{r},\omega_j) := \hat{v}_k(\vec{r},\omega_j)h(d).$$

Here d is the perpendicular distance of the point $\vec{r}$ to the wall. The function $h(d)$ is defined by

$$h(d) = 1 - \exp\left(-(1+\mathrm{i})d/\delta\right),$$

where the viscous penetration depth is

$$\delta = \sqrt{\frac{2\eta}{\rho\omega_j}}.$$

Obviously, this function contains an oscillating and a damping factor. Instead of $\hat{v}_k$ one has to use $\hat{v}_k^*$ in the force term f_l of the Navier-Stokes equation.

3 Implementation

The stationary temperature field that has been calculated as described in section 2.1, is symmetrical with respect to a reflection at the vertical plane which contains the lamp axis. It is sufficient to consider one half of the physical geometry (Figure 3) subject to appropriate symmetry boundary conditions ($\vec{n}\cdot\vec{u} = 0$, $\vec{n}\cdot(-\kappa\vec{\nabla}T) = 0$). In principle one needs the temperature field for AC-operation. In order to save computer time, the corresponding simulations have been performed for direct-current operation. This introduces a certain asymmetry with respect to the $x-z$-plane (see Figure 4) placed in the middle between the electrode tips. To get rid of this asymmetry,s only a quarter of the physical model has been simulated. The fields obtained for this simplified model have been mapped onto the full geometry. In addition, the geometry of the electrodes has been modeled with slight simplifications. For the calculations of the acoustic response function and the streaming field the full geometry has been used. Exemplary, the mesh for the calculation of the streaming field is displayed in Figure 4.

It has been a certain challenge to obtain the distance d mentioned at the end of section 2.3. This has been done by defining a subdomain of thickness $50\ \mu\mathrm{m} \approx 10\delta$ inside the arc tube and adjacent to the wall. On this domain

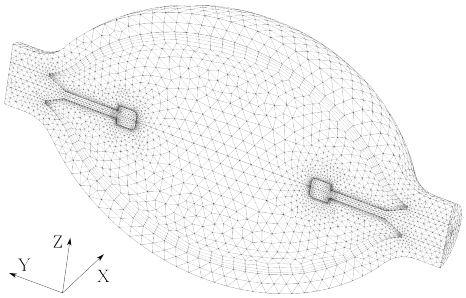

Figure 4: Finite element mesh with boundary layer used for the calculation of the streaming velocity field.

a heat transfer model for solids has been introduced. On the boundary at the wall a zero temperature boundary condition has been implemented and at the opposite boundary the temperature has been set to one. The pseudo temperature resulting as the solution of this heat transfer problem varies across the domain linearly from zero to one and can, after scaling with the proper factor, be used as an estimate of d. The mesh of Figure 4 is too coarse to resolve the function $h(d)$ properly, in particular to resolve the oscillating factor. The important property of this function in the present context is the exponential descent towards the wall of the arc tube. The mesh is fine enough to resolve this descent, albeit only coarsely.

4 Results

In Figure 5 the temperature distribution is depicted. This temperature field serves as input for the calculation of the acoustic eigenmode (Figure 6).

In Figure 7 and the left part of Figure 9 (see appendix) the streaming field associated with the mode in Figure 6 is depicted. A close look at the flow pattern in the top left part of Figure 9 reveals the same structure as the one in Figure 8 - namely two by two vortexes. Figure 8 shows the streaming pattern due to a longitudinal mode in a cylindrical tube. This velocity field has been derived analytically in [14]. The two systems are alike in principle but different in detail. That we observe a similar structure of the flow patterns including the flow direction of all four vortexes indicates that the finite element model works properly.

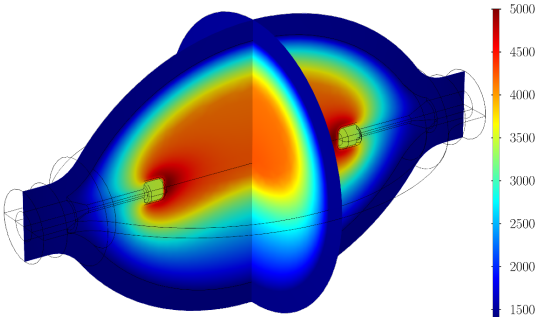

Figure 5: Temperature field. The numbers at the color scale indicate the temperature in K.

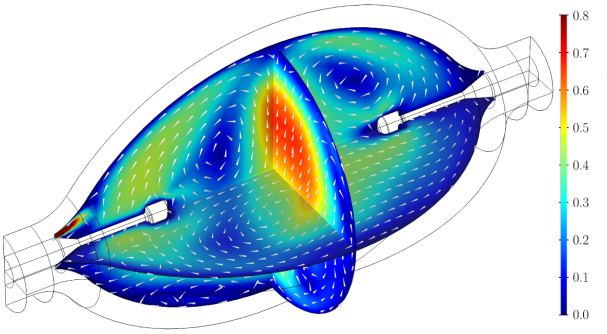

Figure 7: Streaming velocity field. The numbers at the color scale indicate the velocity in $\mathrm{m/s}$.

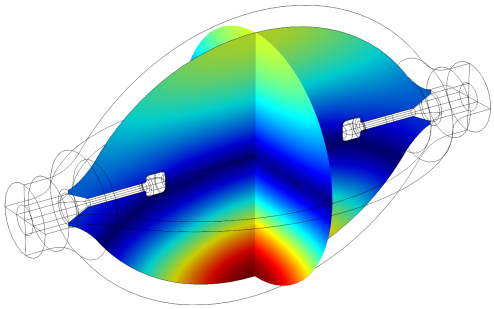

Figure 6: $|p|$ for the 47.4 kHz acoustic pressure mode. The absolute values are of no importance.

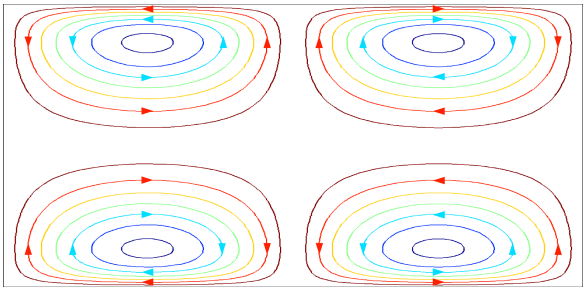

Figure 8: Streaming velocity field resulting from longitudinal modes in a cylinder [14].

From Figure 7 one can see that the maximal streaming velocity is about $0.8\ \mathrm{m/s}$. In [6] a maximal velocity of $1\ \mathrm{m/s}$ is reported. In the 3D model the maximal buoyancy velocity is $7.9\ \mathrm{cm/s}$ and in the 2D model of [6] it is $8\ \mathrm{cm/s}$. Since the investigated lamps are different in respect of geometry, wattage and other properties, this is a very satisfying accordance.

The streaming field dominates over the buoyancy driven flow. It is clear that the physical conditions inside the arc tube will drastically change once streaming sets in. The temperature distribution changes substantially from the original field which has been calculated as described in section 2.1. It is easy to imagine that these violent changes result in arc flicker. In this sense the present model can be used as a tool to investigate if one can expect light flicker under a certain operation condition. Alternatively, one can go one step further. To obtain the correct stationary fields one has to repeat the whole calculations recursively until convergence. The streaming force has to be calculated from the sound particle velocity of the previous step. Once convergence has been obtained, it would be interesting to investigate, whether the resulting flow field is stable or not. This can be accomplished with the aid of a linear stability analysis [15]. We plan to extend our work in this sense in the near future.

The flow pattern depicted in the left part of Figure 9 is obviously not mirror symmetric with respect to the $x-z$-plane (see Figure 4) placed in the middle between the electrode tips. The model itself is completely symmetric and the question arises, how this asymmetry can be explained. It is well known that in nonlinear dynamical systems, like the one under investigation here, symmetry breaking can occur [15]. Famous examples are the Taylor vortexes, which can appear in the gap between rotating cylinders and the Rayleigh-Bénard system. In these systems a symmetry gets lost once a certain control param-

eter rises above a critical value. One can speculate that this happens here. To test this hypotheses, we calculated a series of streaming fields with the force term

$$f_l = \frac{1}{n}\frac{\partial \overline{\rho v_k v_l}}{\partial x_k} - \delta_{l3}\rho g,$$

where $n = 1, 2, 4, 8, ...$ Alternatively, one could shift the AC-frequency away from the resonance frequency. This would be a more physical approach but it is simpler to multiply the first term in f_l by a factor. The result should be the same. In fact the symmetry is restored when the force becomes weaker (Figure 9, right). We conclude that the streaming field suffers symmetry breaking[2]. The similarity of the general structures of the symmetric velocity field with the field of Figure 8 is striking.

5 Conclusions

A stationary 3D finite element model for the calculation of the acoustic streaming field inside the arc tube of HID lamps has been developed. The results obtained with the model are consistent with theoretical expectations. It has been found that the streaming field suffers a symmetry breaking transition with the streaming force as control parameter. Acoustic streaming is assumed to be responsible for light flicker, which is observed when the lamp is operated near an acoustic resonance frequency. The maximal streaming velocity at the investigated resonance is about $0.8\ \mathrm{m/s}$. As this is a large velocity inside a vessel of diameter $6\ \mathrm{mm}$, it does not appear surprising that the plasma arc is severely disturbed by the streaming field.

The acoustic streaming field at other acoustic eigenmodes can be used to stabilize the plasma arc (arc straightening) [16]. The finite element model, which is presented here, should be useful in finding these modes.

6 References

[1] Georges Zissis and Marco Haverlag. Diagnostics for electrical discharge light sources: pushing the limits. *Journal of Physics D: Applied Physics*, 43(23):230301, 2010.

[2] Paul Waide, Satoshi Tanishima, and Phil Harrington. *Light's Labour's Lost: Policies for Energy-efficient Lighting*. OECD, 2006.

[3] The strength and potentials of metal halide lighting systems. Technical report, National Bureau of Standards, Rosslyn, VA, 2010.

[4] Grigoriy A Trestman and Osram Sylvania. Minimizing cost of hid lamp electronic ballast. In *IECON 02 [Industrial Electronics Society, IEEE 2002 28th Annual Conference of the]*, volume 2, pages 1214–1218. IEEE, 2002.

[5] Farhang Afshar. The theory of acoustic resonance and acoustic instability in hid lamps. *Leukos*, 5(1):27–38, 2008.

[6] Thomas D Dreeben. Modelling of fluid-mechanical arc instability in pure-mercury hid lamps. *Journal of Physics D: Applied Physics*, 41(14):144023, 2008.

[7] Jörg Schwieger, Bernd Baumann, Marcus Wolff, Freddy Manders, and Jos Suijker. Influence of thermal conductivity and plasma pressure on temperature distribution and acoustical eigenfrequencies of high-intensity discharge lamps. In *Proc. COMSOL Users Conf.*, Rotterdam, Netherlands, 2013.

[8] Lloyd B Kreuzer. The physics of signal generation and detection. *Optoacoustic Spectroscopy and Detection*, pages 1–25, 1977.

[9] Bernd Baumann, Marcus Wolff, Bernd Kost, and Hinrich Groninga. Finite element calculation of photoacoustic signals. *Applied Optics*, 46(7):1120–1125, 2007.

[10] Bernd Baumann, Marcus Wolff, John Hirsch, Piet Antonis, Sounil Bhosle, and Ricardo Valdivia Barrientos. Finite element estimation of acoustical response functions in hid lamps. *Journal of Physics D: Applied Physics*, 42(22):225209, 2009.

[11] Lord Rayleigh. On the circulation of air observed in Kundt's tubes, and on some allied acoustical problems. *Philosophical Transactions of the Royal Society of London*, 175(0):1–21, 1883.

[2] We plan to investigate this more thoroughly by introducing a number that measures the strength of the asymmetry.

[12] Said Boluriaan and Philip J Morris. Acoustic streaming: from Rayleigh to today. *International Journal of aeroacoustics*, 2(3):255–292, 2003.

[13] Samuel Temkin. *Elements of acoustics*. Wiley New York, 1981.

[14] K Schuster and W Matz. Über stationäre Strömungen im Kundtschen Rohr. *Akustische Zeitschrift*, 5:349–352, 1940.

[15] Michael Cross and Henry Greenside. *Pattern formation and dynamics in nonequilibrium systems*. Cambridge University Press, 2009.

[16] Jo Olsen and Thomas D Dreeben. Experimental and simulated straightening of metal halide arcs using power modulation. *Industry Applications, IEEE Transactions on*, 47(1):368–375, 2011.

[17] Philips material database. Technical report, Philips.

[18] Jerome G Hust and Alan B Lankford. Update of thermal conductivity and electrical resistivity of electrolytic iron, tungsten and stainless steel. *U. S. Dept. of Commerce*, page 61, 1984.

7 Acknowledgments

This research was supported by the German Federal Ministry of Education and Research (BMBF) under project reference 03FH025PX2 and Philips Lighting.

8 Appendix

Electric conductivity σ	see Figure 2	[7]
Density ρ	$\frac{PM}{R_\mathrm{m}T}$	
Static pressure P	$2.81\ \mathrm{MPa}$	
Molar mass M	linear function of T through the points $191\ \mathrm{g/mol}$ at $1450\,\mathrm{K}$ and $184\ \mathrm{g/mol}$ at $5800\,\mathrm{K}$	[17]
Viscosity η	see Figure 2	[17]
Thermal conductivity κ of ...		
... arc filling	see Figure 2	[17]
... tungsten	according to literature	[18]
... PCA	$(0.0378 - 556 \cdot 10^{-7}\Delta T$ ... ... $+282 \cdot 10^{-10}\Delta T^2) \cdot 10^3\,\frac{\mathrm{W}}{\mathrm{m\,K}}$ with $\Delta T = T - 273.15\,\mathrm{K}$	[17]
Specific heat capacity at constant pressure c_p	linear function of T through the points $111\ \mathrm{J/(kg\,K)}$ at $1450\,\mathrm{K}$ and $115\ \mathrm{J/(kg\,K)}$ at $5800\,\mathrm{K}$	
Power loss due to radiation q_rad	see Figure 2	[17]
Temperature at electrode ground T_0	$1430\ \mathrm{K}$	
Emissivity of PCA	$\epsilon = \frac{(110\,t+19)\cdot 10^{12}}{T^5} + 0.195 - \frac{0.017}{t}$ with $t = 0.5\ \mathrm{mm}$ (thickness of arc tube wall)	[17]
Ambient temperature T_amb	$293\ \mathrm{K}$	
Current density J_0	$0.548\ \mathrm{A/mm^2}$	
Specific heat ratio γ	1.4	
Speed of sound c	$\sqrt{\frac{\gamma R_\mathrm{m} T}{M}}$	

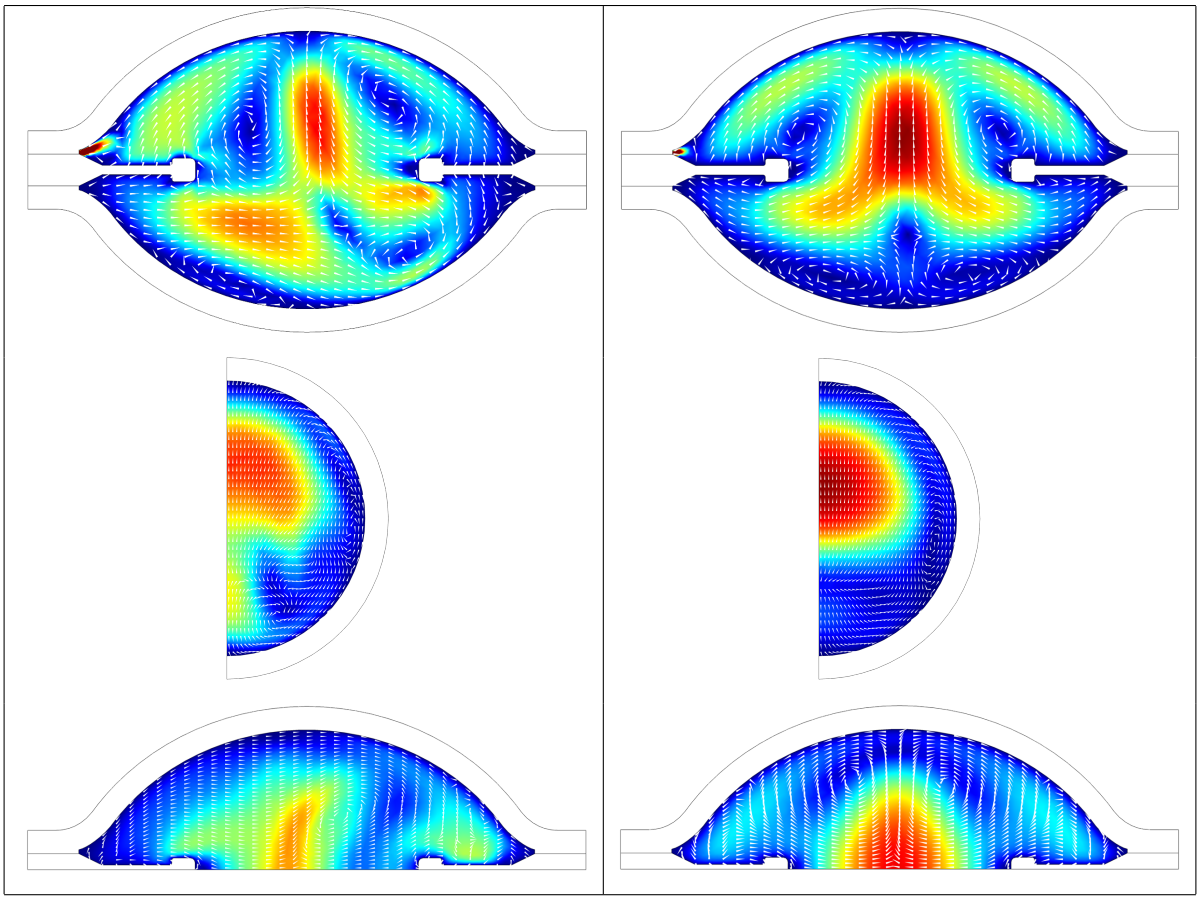

Figure 9: Left: Streaming velocity field with full streaming force ($n = 1$). Right: Streaming velocity field obtained with down-scaled streaming force term ($n = 8$). For $n = 8$ the maximal streaming force exceeds the maximal buoyancy force by a factor of about 5. The three planes from Figure 7 are depicted separately. Top and middle: Vertical planes, bottom: Horizontal plane. The figures on the top and the bottom of the rhs are almost symmetrical.